

Investigation of the overvoltage and fast transient phenomena on transformer terminals by taking into account the grounding effects

Popov, M; Grcev, L; Høidalen, KR

DOI

[10.1109/TIA.2015.2411652](https://doi.org/10.1109/TIA.2015.2411652)

Publication date

2015

Published in

IEEE Transactions on Industry Applications

Citation (APA)

Popov, M., Grcev, L., & Høidalen, KR. (2015). Investigation of the overvoltage and fast transient phenomena on transformer terminals by taking into account the grounding effects. *IEEE Transactions on Industry Applications*, 51(6), 5218-5227. <https://doi.org/10.1109/TIA.2015.2411652>

Important note

To cite this publication, please use the final published version (if applicable). Please check the document version above.

Copyright

Other than for strictly personal use, it is not permitted to download, forward or distribute the text or part of it, without the consent of the author(s) and/or copyright holder(s), unless the work is under an open content license such as Creative Commons.

Takedown policy

Please contact us and provide details if you believe this document breaches copyrights. We will remove access to the work immediately and investigate your claim.

Investigation of the Overvoltage and Fast Transient Phenomena on Transformer Terminals by Taking into Account the Grounding Effects

Marjan Popov

Senior Member, IEEE
Delft University of
Technology
Faculty of EEMCS,
Mekelweg 4, Delft,
The Netherlands
M.Popov@ieee.org

Leonid Grčev

Fellow, IEEE
University St Cyril and
Methodius
Faculty of Electrical
Engineering, Skopje
R. Macedonia
Leonid.Grcev@ieee.org

Hans Kr.

Høidalen

Senior Member, IEEE
NTNU-Trondheim
Norway
Hans.Hoidalen@elkraft.
ntnu.no

Bjørn Gustavsen

Fellow, IEEE
Sintef Energy
Trondheim, Norway
Bjorn.Gustavsen@sintef.no

Vladimir

Terzija

Senior Member, IEEE
The University of
Manchester, UK
terzija@ieee.org

Abstract – A large number of electromagnetic transient studies have so far reported findings related to the overvoltage behaviour of systems within a broad frequency range. However, in most cases, actual grounding effects have been either not taken into account or have been just partially considered. Although an accurate methodology to study grounding effects exists, a detailed analysis of the grounding effects has not yet been fully performed. Besides, many test applications are performed in laboratories where the grounding is close to ideal. In this paper, the grounding system modelling methodology is described and its capability is demonstrated for an existing complex grounding system. Firstly, the complex grounding system is modelled in frequency domain by the TRAGSYS program, which represents the grounding system as an equivalent multi-port network. Next, the equivalent network parameters are represented in a broad frequency range enabling time domain computations in ATP-EMTP. Finally, the protection level of the chosen lightning arresters is discussed under most severe conditions.

Index Terms– ATP-EMTP, electromagnetic modeling, grounding, lightning arresters, transients, transformers, protection.

I. NOMENCLATURE

m, n – segments in the grounding mesh
 I_n – current in a specific segment of the grounding mesh
 U_n – induced voltage in the n -th segment
 Z_{Smn} – mutual impedance between nodes m and n
 $D, E, \underline{c}_n, \underline{a}_n$ – parameters of the polynomial expression

II. INTRODUCTION

Power systems are designed to produce, transmit and distribute electricity to the remote consumers economically and in a secure manner. To achieve that, power systems are grounded at specific points. These are normally generator and transformer neutral points, which actually represent the system grounding. In this way, the ground serves as a return path for the fault currents with a resistance that should be kept as low as possible. However, it is of greatest importance that such a low ground resistance should help in decreasing the potentials during faults and other disturbances. Therefore, the goal of the grounding is twofold: 1) to provide safety against electric shock resulting from step and touch voltages for the people in the vicinity of the electrical equipment, 2) to provide correct operation of the power system, e.g. providing correct level of fault currents important for the operation of power system protection.

First issue is related to the safety of the people working in the environment of the grounding system or using electrical apparatus. This is well elaborated so far [1]-[5]. In order to achieve this, substation and power plant grounding systems are usually

complex grounding structures that consist of meshes in a form of horizontally interconnected conductors, which sometimes are supplied with vertical rods. The second issue, however, deals with the system grounding and during normal power system operation, the grounding impedance is predominantly resistive and straightforward to be determined. The grounding system in this case is close to an ideal grounding and the grounding effect can be easily included into the self- and mutual impedances of lines and cables that further determine the symmetrical component values of the transmission and distribution system [6]. However, for fast transient oscillations that occur during lightning, disconnecting lines, cables, transformers and switchgear in GIS, grounding system performance is quite different. Grounding impedance is frequency dependent and in case of high intensity currents, it may be non-linear due to earth ionization [7]. Such complex behavior of grounding systems during fast transients might enhance the overvoltages and might degrade overvoltage protection applied on the system. This effect is usually not taken into account in test laboratories that perform their test duties in a laboratory environment where equipment is grounded at one point so that the effect of the grounding is minimized.

The complex transient behavior combined with complex geometry of the grounding structures makes the modeling of the grounding system for power system transient studies very complicated. Recently, models based on the rigorous full wave electromagnetic theory that are thoroughly tested by comparison with experiments have been described [8]-[10]. The application of these mathematically complex models is recently utilized by software with simple graphical interface, such as TRAGSYS [10]. In this paper, we have used TRAGSYS program to extract equivalent network parameters from the electromagnetic model of the grounding system. Such network equivalents enable direct representation in complete system transient analysis using ATP-EMTP. Accurate computation of fast transients is very important for insulation coordination and equipment design. In this paper, it is proven that during fast transients, the effect of the grounding system highly influences the overvoltages, which depending on the distance between the overvoltage protection and the transformer may exceed the Basic Insulation Level (BIL) of the transformer.

In this paper for the first time we have enhanced the accuracy of computations by coupling more sophisticated models of components like transformers and lightning arresters. All models are frequency dependent, which is important for accurate representation of the residual voltages after a lightning arrester operates. The transformer is very accurately represented so that

the potentials of both the transformer and the arrester neutral point can be computed very accurately.

The paper is organized in the following way. Chapter III explains the approach of complex grounding system model. Chapter IV describes the methodology applied to interface the complex grounding system to the network. Chapter V deals with the comparison of the computed results by TRAGSYS and ATP-EMTP. Chapter VI describes the studied system and associated component modeling with a special focus on the lightning arrester model. Chapters VII and VIII deal with the simulated results and conclusion respectively.

III. MODELING COMPLEX GROUNDING SYSTEMS

The analysis is in frequency domain, that is, the response of a steady-state time-harmonic excitation computed for a wide frequency range. Interested reader may find full details on the underlying theory of the model in [8], [9]. Here, we briefly describe the basic step in the modeling process. The physical model of the grounding system is assumed to be a network of straight cylindrical metallic conductors with arbitrary orientation. A suitable equivalent radius is assumed in the case when conductor's cross section is not circular. It is assumed that the conductor length is much greater than the radius which is much smaller than the wavelength of the medium (in practice ratio of 10 is usually satisfactory). This assumption enables so called thin-wire approximation by which the total current in the conductors is represented by filamentary line current in the conductors' axis. We consider the grounding system detached from the above ground system and completely buried in the earth. In the present analysis, we assume a homogenous model of soil characterized by apparent conductivity and permittivity constants. The case in which the soil is layered with different characteristics of layers will be considered in later work.

The basic goal of the modeling is to determine the longitudinal current distribution along conductors in the grounding system. The first step in analysis is to divide the grounding conductors in fictitious segments (all segments must be subject of thin-wire approximation). Fig. 1 illustrates such a division in fictitious segments. They can have variable length which is numbered appropriately. We distinguish segments with open ends in which a current is injected. These segments are numbered by $m = 1, 2, \dots, M$ and shown with encircled numbers in Fig. 1. All the other segments are numbered separately by $n = 1, 2, \dots, N$. The next step is to assume a longitudinal current distribution along a segment. The simplest approximation is to assume a constant distribution [8]. Another possibility for approximation of the current along segments is described in [9]. In such a case, the current along the n -th segment is

$$I(l) = I_n F_n(l) \quad (1)$$

where $F_n(l)$ is equal to one for the n -th segment and zero elsewhere. Here, I_n is the phasor that determines the current at the n -th segment.

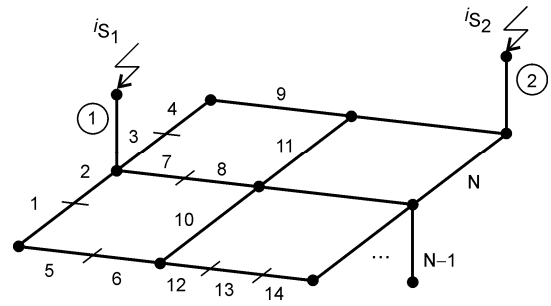


Fig. 1. Grounding system model divided in fictitious segments.

Therefore, the current distribution along conductors is approximated by a stepwise approximation I

$$I(l) = \sum_{n=1}^N I_n F_n(l) \quad (2)$$

The goal of this analysis is to determine the unknown I_n . Fig. 2 illustrates the actual longitudinal current and its stepwise approximation.

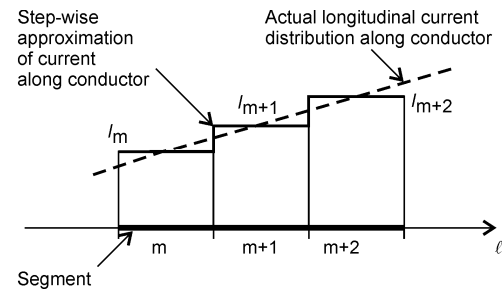


Figure 2. Actual longitudinal current distribution along conductor axis and its stepwise approximation.

Since the current flows from the conductors into the soil, the longitudinal current is variable along the conductors. It is clear that the accuracy of the approximation depends on the total number of segments N ; larger number (and smaller) segments leads to an increased accuracy. The next step is to determine electromagnetic interaction between segments. Here, we distinguish M segments with shunt excitation (by injection of current) and the other N segments that can have serial excitation. We assume that such serial excitation can be applied by an ideal current or voltage generator connected between an infinitesimal gap at the segment center. Therefore, we assume that there exists a two-terminal port at the center of the segment, which is short circuited when there is no serial excitation. First, we consider two segments with a serial excitation and denote them by 'm' and 'n' in Fig. 3(a). If an ideal current generator with a current I_m is applied, a constant current is impressed along the n -th segment. Next we can determine the resulting electric field \vec{E}_n at the surface along the n -th segment. The induced voltage U_n along the n -th segment is obtained by integrating the tangential component of \vec{E}_n . The electromagnetic interaction between the segments is determined by the generalized impedances [11]:

$$z_{mn} = \frac{U_n}{I_m}, \quad n = 1, 2, \dots, N, \quad m = 1, 2, \dots, N \quad (3)$$

Similarly, the mutual impedance between a segment with a shunt excitation (current injection) and another segment is:

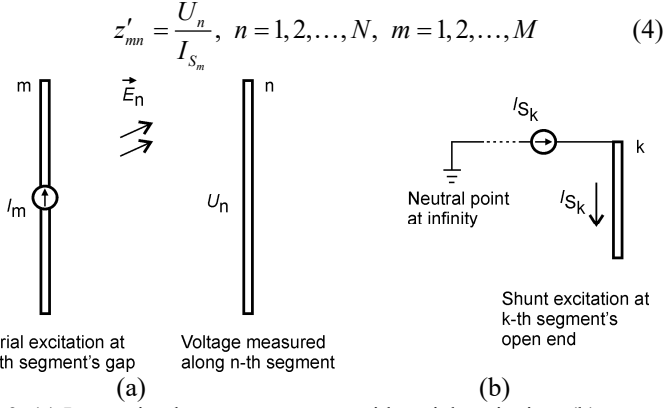


Fig. 3. (a) Interaction between segments with serial excitation; (b) Segment with shunt excitation.

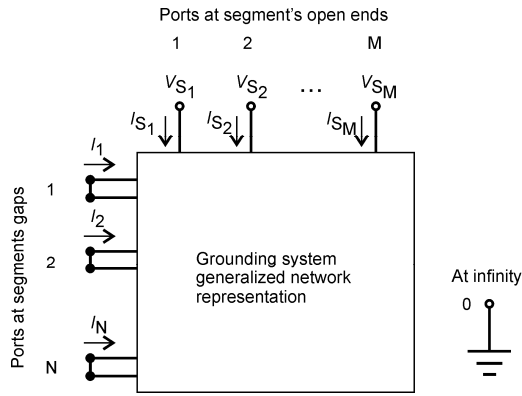


Fig. 4. Generalized network representation of the grounding system

This is equivalent to a network representation of the grounding system where N two-terminal ports are at the infinitesimal gaps at the segments' center, while M one-terminal ports correspond to segments where current injection is applied (the other terminal of these ports is at a neutral point – theoretically at infinity), Fig. 4. Segments gap ports are short-circuited in the normal operation, but they can be used to simulate impressed serial excitation when the grounding structure is under influence of an external field. We consider that the grounding system excitation consists of M ideal current generators with currents $I_{S_k}, k=1,2,\dots,M$ connected between the one-terminal ports and the neutral point at infinity (the influence of the connecting cables is neglected). Based on the linearity and the superposition principle, the interaction between all segments is described by the matrix equation [12]:

$$\begin{bmatrix} z_{11} & z_{12} & \dots & z_{1N} \\ z_{21} & z_{22} & \dots & z_{2N} \\ \vdots & \vdots & \ddots & \vdots \\ z_{N1} & z_{N2} & \dots & z_{NN} \end{bmatrix} \cdot \begin{bmatrix} I_1 \\ I_2 \\ \vdots \\ I_N \end{bmatrix} = \begin{bmatrix} z'_{11}I_{S_1} + z'_{12}I_{S_2} + \dots + z'_{1M}I_{S_M} \\ z'_{21}I_{S_1} + z'_{22}I_{S_2} + \dots + z'_{2M}I_{S_M} \\ \vdots \\ z'_{N1}I_{S_1} + z'_{N2}I_{S_2} + \dots + z'_{NM}I_{S_M} \end{bmatrix} \quad (4)$$

The solution of (4) provides the coefficients I_m for N segments

$$[I] = [z]^{-1} \cdot \{I_{S_1}[z'_1] + I_{S_2}[z'_2] + \dots + I_{S_M}[z'_M]\} \quad (5)$$

and therefore the longitudinal current distribution (2) along all conductors of the grounding system. When the currents are known, all other quantities of interest such as: fields, potentials,

voltages, impedances, can be straightforwardly computed.

IV. INTERFACE TO TRANSIENT PROGRAMS

The M ports at segments' open ends are connecting points to the power system. The interface to the power system is based on impedances seen from and between these M ports. The self- and mutual grounding harmonic impedance seen from and between M ports at segments open ends are

$$Z_{S_{mn}} = \frac{V_{S_m}}{I_{S_n}} = \frac{[I]^T [z'_n] + I_{S_n} z'_{S_{mn}}}{I_{S_n}}, \quad m=1,2,\dots,M, \quad n=1,2,\dots,M \quad (6)$$

All quantities to determine $Z_{S_{mn}}$ in (6) are already evaluated by (5), except $z'_{S_{mn}}$, which are mutual impedances between shunt excitation segments 'm' and 'n'.

Therefore we have reduced the order of the network representation of the grounding system from $N+M$ in (4) to M

$$[V_S] = [Z_S] \cdot [I_S]. \quad (7)$$

The equivalent circuit seen from the above grounding system is illustrated in Fig. 5. The next step is to approximate $Z_{S_{mn}}$

represented by a linear approximation by vector fitting procedure and/or aramfit. Transient programs like ATP-EMTP are capable of dealing with circuits as those presented in Fig. 5. By making use of the powerful user-defined Tacs/Models, current-controlled voltage sources are programmed in Models, whereas the self-impedance is synthesized and applied directly in ATP-EMTP.

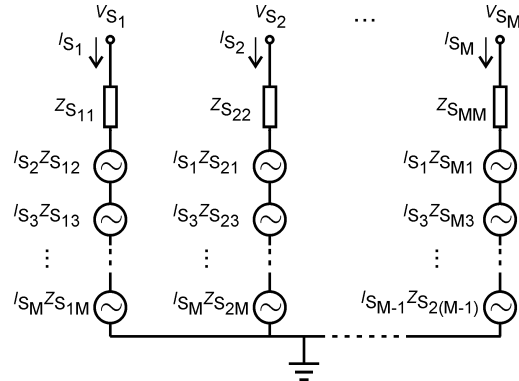


Fig. 5. A grounding system equivalent circuit seen from the above ground power system.

In order to represent the grounding system accurately, the impedances from equation (7) needs to be fitted within a broad frequency range. So far, there was a lot of work done on synthesizing frequency dependent characteristics by electric circuits. In [13], it was provided an efficient method to represent the impedance characteristic within broad frequency range. This is valid only for self-impedances.

There were different methods investigated to find the most appropriate way of representing these impedances. It was found that the self-impedances of the $Z_{S_{mn}}$ fitted by making use of the Aramfit approach [14],[15] are very efficient to represent the impedance within broad frequency range. Moreover, this approach provides the coefficients of a rational function known as Kizilcay F-dependent [16], which is directly implementable in ATP-EMTP environment. Off-diagonal impedances are fitted by making use of the vector fitting approach [17]. In this way, the fitting of the characteristics is obtained with high accuracy. Furthermore, the

off-diagonal elements are expressed in partial fractions since they need to be multiplied by the current that is provided from the power system simulated in ATP-EMTP. As an output, the computed voltage is provided, which is exported to type-60 current-controlled voltage source. The fitted characteristics is expressed by:

$$Z_{S_{mn}}(s) = D + sE + \sum_{n=1}^{N_p} \frac{c_n}{s - \underline{a}_n} \quad (8)$$

where N_p is a positive integer, $s = j\omega$. D and E are real whereas c_n and \underline{a}_n could be either real and/or a pair of complex conjugated numbers, which can be represented as a second order polynomial partial fraction with real constant parameters. In this way, it is possible to represent the expressions in Models by making use of the Laplace function. Alternatively, the fitting of the whole matrix $Z(s)$ can be done by vector fitting. The use of both, gives opportunity to use also embedded models of ATP-EMTP like Kizilcay F-Dependent.

V. MODEL VALIDATION

A. Validation of the computed impedance characteristics

The above described procedure is applied on a grounding system with dimensions 60mx60m. In this case, the impedance frequency characteristics are determined by the electromagnetic model and fitted accordingly. Fig. 6 shows the results of the synthesized characteristics for a feeding point at the lightning arrester location AA. For this case, a lightning impulse of 10 kA, 1.2/50 μ s has been injected at AA and the corresponding voltage has been computed. Fig. 7 shows the results of the ground potential rise at the same point where the current is injected. It can be seen that the ATP-EMTP model shows very good matching with the electromagnetic model.

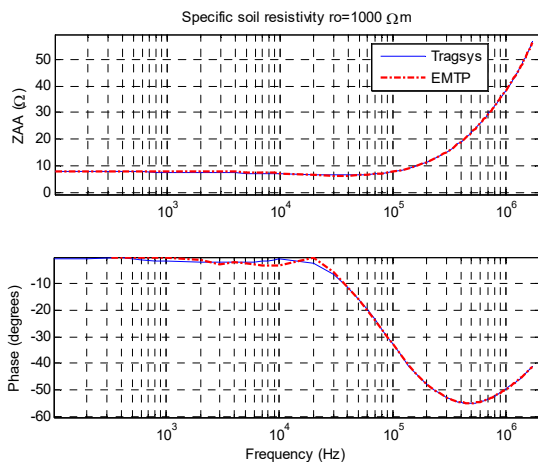


Fig. 6. Amplitude and phase characteristic of the impedance Z_{AA} at the arrester grounding point of the grounding system, for the soil resistivity of 1000 Ω m.

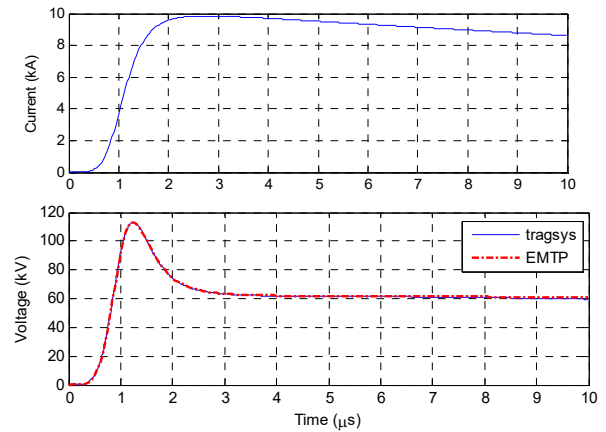


Fig. 7. Current impulse 1.2/50 μ s and corresponding ground potential rise at the arrester grounding point.

Figs 8 and 9 show results for a case when the lightning occurs at the point M located in the middle of the grounding system. Fig. 8 is the impedance characteristic of the grounding system seen from the point M for a characteristic soil resistivity of 1000 Ω m.

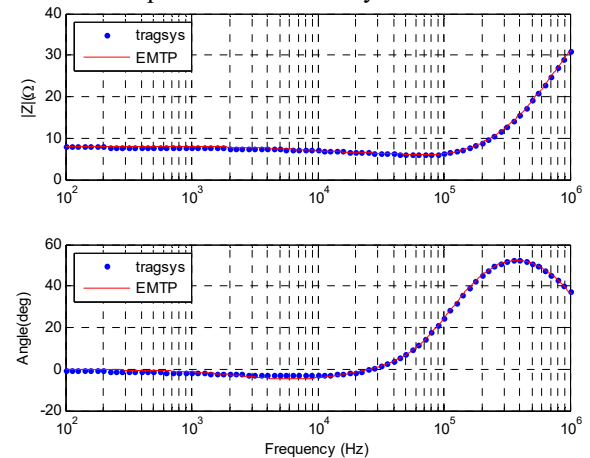


Fig. 8. Amplitude and phase characteristic of the impedance Z_{MM} in the middle of the grounding system.

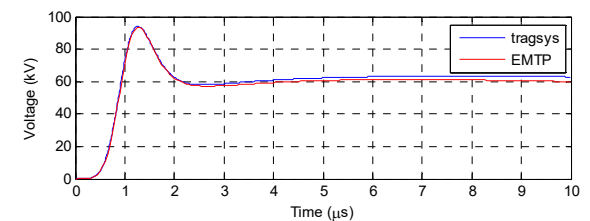


Fig. 9. Ground potential rise in the middle of the grounding system.

Fig. 9 shows the corresponding ground potential rise when a lightning stroke is injected in the middle of the grounding systems.

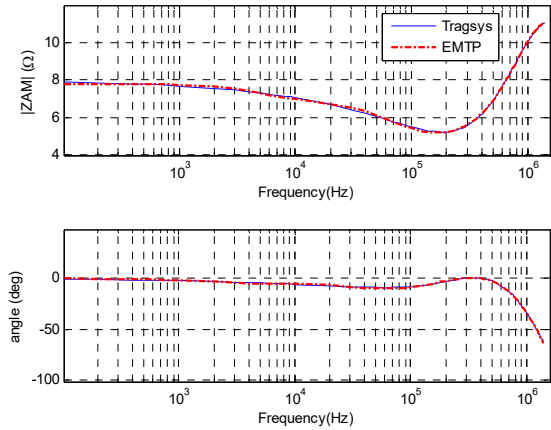


Fig. 10. Amplitude and phase characteristic of the mutual impedance Z_{AM} between the arrester earthing point AA and the middle point MM of the grounding system for a specific soil resistivity of 1000 Ωm .

Figs. 10 and 11 present the results of the mutual impedance characteristics between the arrester grounding point and the middle point, and the corresponding ground potential rise. Fig. 11 shows the voltage rise at the arrester earthing point when the lightning is injected in the middle point of the grounding system. It can be seen that the last case differs significantly with respect to the previous case. The voltage rise is delayed by approximately a half of a microsecond.

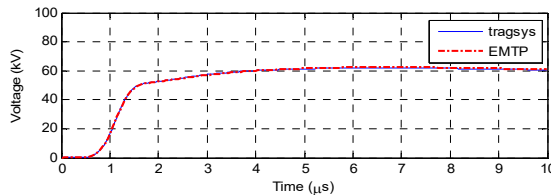


Fig. 11. Ground potential rise at the arrester grounding point when the lightning stroke is injected in the middle point the grounding system.

Accordingly, the impedance characteristics are fitted for a specific resistivity of 100 Ωm and time domain voltage responses are verified in the same way.

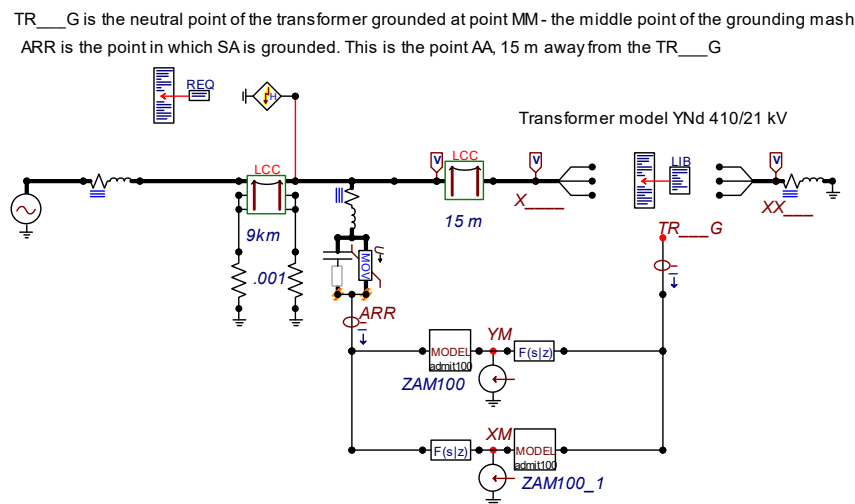


Fig. 13. Representation of the studied system modelling in ATPDraw.

A. Lightning arrester modelling

The choice of the lightning arrester is made according to the nominal system voltage and the corresponding Maximum Continuous Overvoltage U_c . Besides, it is also recommended to

VI. STUDIED SYSTEM

The analysis is performed for a 420 kV network as illustrated in Fig. 12. The system that consists of an overhead line connecting a 434/21 kV power transformer with a BIL of 1425 kV. The transformer is protected by lightning arresters installed 15 m away from the transformer. The grounding system is a 60m x 60m grid consisting of 10m x 10m meshes constructed from copper conductors with a diameter 1.4 cm, buried at 0.5 m depth. The soil is homogeneous with resistivity 100 Ωm , relative permittivity 10 and permeability of air.

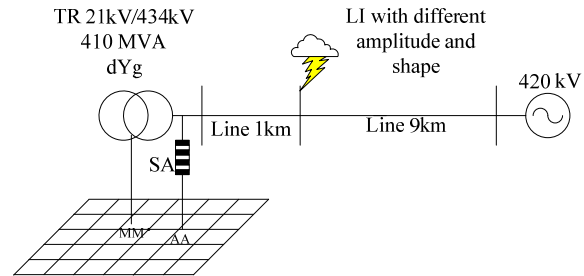


Figure 12. An illustration of the studied system.

The overhead line is modeled by ATP's J-Marti frequency-dependent transmission line model. The 15 m connection between the lightning arresters and the transformer is also modeled by J-Marti routine. Refined models for the lightning arresters and the transformer are applied as detailed in the following subsections. All models are implemented in ATPDraw environment as shown in Fig. 13. The overhead line consists of two conductors per phase and is equipped with ground wires. In this study, we consider a worst-case scenario with the lightning strike directly to a phase wires without any flashover along the line. Ground wires in this case are also not connected to the studied grounding system.

pay attention to the line discharge class, which is related to the absorbed arrester energy. According to [19], a PEXLIM Q arrester of class 3 with 7.8 kJ/kV with a rated voltage $U_r = 336$ kV and $U_c = 267$ kV has been chosen. The U-I characteristic for this

arrester is determined by making use of [20] and is shown in Fig. 14.

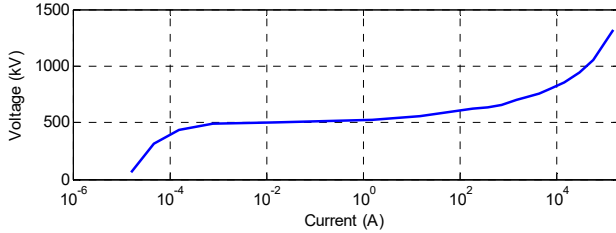


Fig. 14. Lightning arrester characteristic.

For high frequencies however, corresponding to impulses with a short front of wave, the variable resistance computed according to Fig. 14 is not enough. Therefore, a frequency dependent arrester model is applied [21]. The non-linear resistance computed from Fig. 14 is connected in parallel with a capacitor of 0.3 nF and this parallel connection is connected in series with an R-L branch 1 mΩ and 1μH. With these data, a satisfactory results can be achieved, which are close to the catalogue data. Fig. 15 summarizes the results of the applied model for different impulses. For 10 kA, 20 kA and 40 kA with a waveform 8/20 μs the model results in 820 kV, 890 kV and 990 kV respectively. These values are slightly higher than those provided in the catalogue, which are 790 kV, 869 kV and 972 kV. For an impulse 10kA, 1.2/50 μs, the computed value is 822 kV. These data are not provided in the catalogue but the experience shows that the voltage is 5-8 % higher than that with an impulse of 8/20 μs, which in this case results between 830-855 kV.

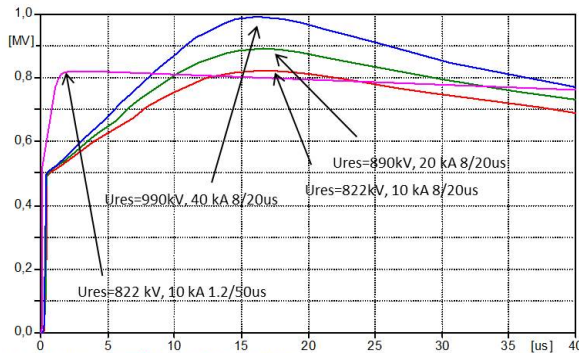


Fig. 15. Results of the residual voltages for different wave shapes.

B. Transformer modelling

The transformer is represented by a frequency-dependent model on the form (8). The model is obtained from frequency sweep measurements of the 6x6 transformer terminal admittance which are subjected to model extraction using vector fitting and passivity enforcement. More details about the modelling of this transformer and the model performance can be found in [22]. The model is included in ATP-EMTP environment using an equivalent electrical circuit which is generated directly from the pole-residue model.

Although the measurements were only available up to 200 kHz, the transformer model will in this work be used in an application involving higher frequencies.. This could slightly affect the final results, however, more measurements about the transformer at the time when this work was done, could not be provided. On the other hand, the surged voltages strongly depend on the rest of the network and especially the calculated residual voltages of the lightning arrester as well as the impedance terminal characteristic

of the grounding system itself [23], which in this work are provided with great accuracy as previously described.

VII. RESULTS

Based on the performed modeling and system data, an extensive analysis has been carried out in order to see how different lightning impulses affect the lightning arrester with respect to the generated overvoltages. It is also paid attention to see the effect of different values of specific soil resistivity as well as under which conditions, the terminal transformer voltage exceeds the transformer BIL. For all cases, lightning arrester distance from the transformer is kept fixed to 15 m. A change of this parameter implies that the new value of Z_{AA} and Z_{AM} should be recomputed and included. This is not done, because it is actually known that the longer the distance between the lightning arrester and transformer, the higher the overvoltages [5]. Besides, the neutral points of the lightning arresters for all three phases in this study are considered grounded in one point. This is done for two reasons. The first reason is that only two current injections from power system are applied (transformer grounding and the arrester grounding), which requires fewer characteristics to be included.

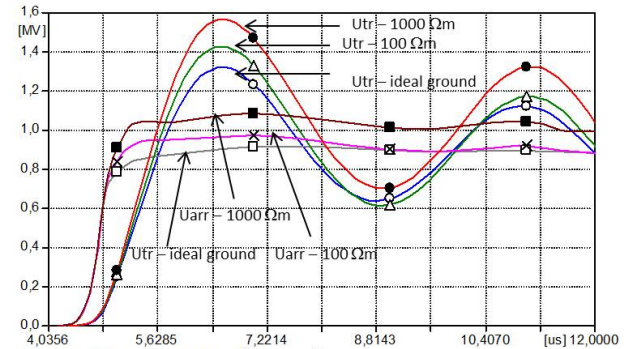


Fig. 16. Comparison between transformer voltages for different specific soil resistivity and ideal grounding for a discharge current 25 kA, 1.2/50 μs.

This simplifies the computation procedure, which even with two current injection points is rather complicated. The second reason is that these points in practice will be very close to each other and will result in low impedances, which do not change the ground potential rise and terminal arrester voltages very much. The performed analysis shows that for the selected grounding system, the specific resistivity plays an important role. Fig. 16 shows that when the grounding is considered as ideal, for a discharge current 25 kA, 1.2/50 μs, the transformer terminal voltage is about 1.3 MV and the arrester terminal voltage is around 900 kV. However, when the specific resistivity is 100 Ωm and 1000 Ωm, transformer terminal voltages rises above 1.4 MV exceeding the transformer BIL. The residual arrester voltages rise accordingly and this is caused by the higher ground potential rise of the arrester grounding point. Fig. 17 shows an example when the system is exposed to a lightning with a 30 kA and a front of wave 0.5 μs, which is shorter than that in the previous case. In this case, the tail of the lightning impulse is 3μs, which is much shorter than that in the previous case. It can be seen that for a specific resistivity of 100 Ωm, this case results in a transformer overvoltage much higher than the transformer BIL. These examples and the rest of the examples of the performed study deal with lightning strokes that take place at the lightning arrester, very close to the substation where the transformer is located. However, one should

be aware that overvoltages that propagate along the lines are much higher than these values. This is demonstrated in Fig. 18, which shows the result of a case when the lightning occurs 1 km away from the arrester location. This example demonstrates the travelling wave phenomena and worst case scenario; it is considered that the lightning hits the phase conductors (even though the line is supplied by ground wires). The possible flashover because of the very high overvoltage is also not taken into account.



Fig. 17. Voltage response when the system is exposed to LI, 0.5/3 us, 30 kA, 100 Ω m.

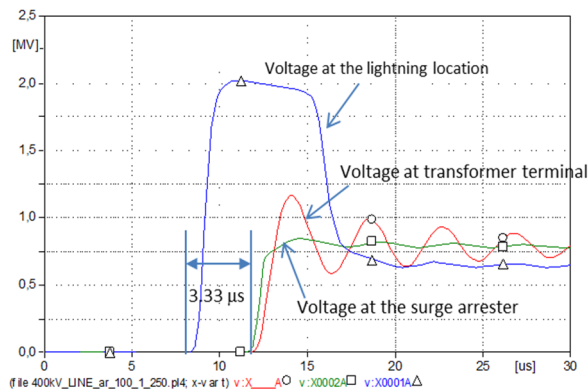


Fig. 18. Overvoltages on the lightning arrester and transformer terminals when the lightning with 10 kA, 1.2/50 μ s occurs on 1 km distance from the transformer.

Since the speed of wave propagation in overhead lines is close to the speed of light, wave travel time from the place where the lightning occurs to the lightning arrester terminals is $1\text{km} / 3e5\text{km/s} = 3.3 \mu\text{s}$. Within this very short period of time, the overvoltage rises to a very high value, which in this case is around 2 MV. Upon reflection from the lightning arrester, the voltage is surged to a value of approximately 830 kV, which corresponds well to the residual voltage of the catalog data. It can be seen that the voltage at the transformer terminals starts rising shortly after the arrester terminals are reached. This is approximately 50 ns, which is equal to the wave travel time from the arrester terminals to the transformer terminals. Tables 1-4 summarizes the results of the computed overvoltages at the arrester and transformer terminals for different specific soil resistivity and lightning currents as well as different lightning wave shapes. It can be seen that longer tails of the lightning impulses result in more discharge arrester current. Besides, in all cases, for a particular lightning impulse, higher specific soil resistivity results in higher transformer terminal overvoltage. For lightning impulses for which front times are longer, BIL is even not achieved when the

lightning current is 50 kA. However, higher specific resistivity significantly influences the residual voltage of the lightning arrester. For example, according to Table 1, for a lightning current of 25 kA and a specific resistivity of 100 Ω m and 1000 Ω m, the residual voltage of the lightning arrester is 973 kV and 1084 kV respectively. This can be well seen in Fig. 16. The difference of the residual voltage also affects the terminal transformer overvoltages, which in this case for both values of the soil resistivity exceed the predefined transformer BIL.

Table 1. Computed results for a LI 1.2/50 μ s.

| R (Ω m) | Is (kA) | Iarr (kA) | Uarr (kV) | Utr(kV) |
|-----------------|---------|-----------|-----------|---------|
| 100 | 10 | 9.46 | 846 | 1170 |
| 100 | 20 | 20.2 | 935 | 1355 |
| 100 | 25 | 25.4 | 973 | 1425 |
| 1000 | 10 | 10 | 874 | 1226 |
| 1000 | 20 | 20.2 | 1025 | 1464 |
| 1000 | 25 | 25.2 | 1084 | 1566 |

Table 2. Computed results for a LI 0.5/3 μ s

| R (Ω m) | Is (kA) | Iarr (kA) | Uarr (kV) | Utr(kV) |
|-----------------|---------|-----------|-----------|---------|
| 100 | 10 | 5.6 | 800.7 | 1157 |
| 100 | 20 | 13 | 948 | 1324 |
| 100 | 25 | 17.5 | 1030 | 1388 |
| 1000 | 10 | 5.6 | 844 | 1184 |
| 1000 | 20 | 12.5 | 1115 | 1395 |
| 1000 | 25 | 17.1 | 1232 | 1484 |

Table 3. Computed results for a LI 0.5/50 μ s.

| R (Ω m) | Is (kA) | Iarr (kA) | Uarr (kV) | Utr(kV) |
|-----------------|---------|-----------|-----------|---------|
| 100 | 10 | 10 | 844 | 1194 |
| 100 | 20 | 20 | 949 | 1368 |
| 100 | 25 | 25 | 1029 | 1433 |
| 1000 | 10 | 9.9 | 888 | 1238 |
| 1000 | 20 | 20 | 1076 | 1468 |
| 1000 | 25 | 25 | 1181 | 1568 |

Table 4. Computed results for a LI 4/10 μ s.

| R (Ω m) | Is (kA) | Iarr (kA) | Uarr (kV) | Utr (kV) |
|-----------------|---------|-----------|-----------|----------|
| 100 | 20 | 18.2 | 918 | 1091 |
| 100 | 50 | 46.7 | 1112 | 1243 |
| 100 | 100 | 96.2 | 1381 | 1415 |
| 1000 | 20 | 18.2 | 998 | 1163 |
| 1000 | 50 | 46.4 | 1316 | 1405 |
| 1000 | 100 | 95.3 | 1810 | 1805 |

The discharge current through the lightning arresters is large when the arrester operates and causes high ground potential rise. Fig. 19 shows a comparison between the ground potential rise computed by TRAGSYS and ATP-EMTP. This is also a verification that the interface of the whole grounding system is well done in ATP-EMTP environment.

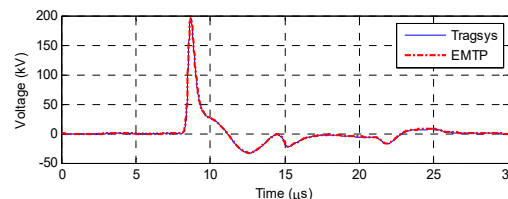


Fig. 19. Voltage at the arrester grounding point AA computed by Tragsys and EMTP for the case 30 kA 0.5/3 μ s and soil resistivity 100 Ω m.

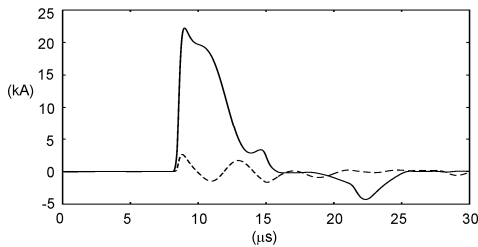


Fig. 20. Current injected into the grounding system for the case of lightning current of 30 kA 0.5/3 μ s and soil resistivity 100 Ω m. Full line – at arrester grounding point. Broken line – at transformer.

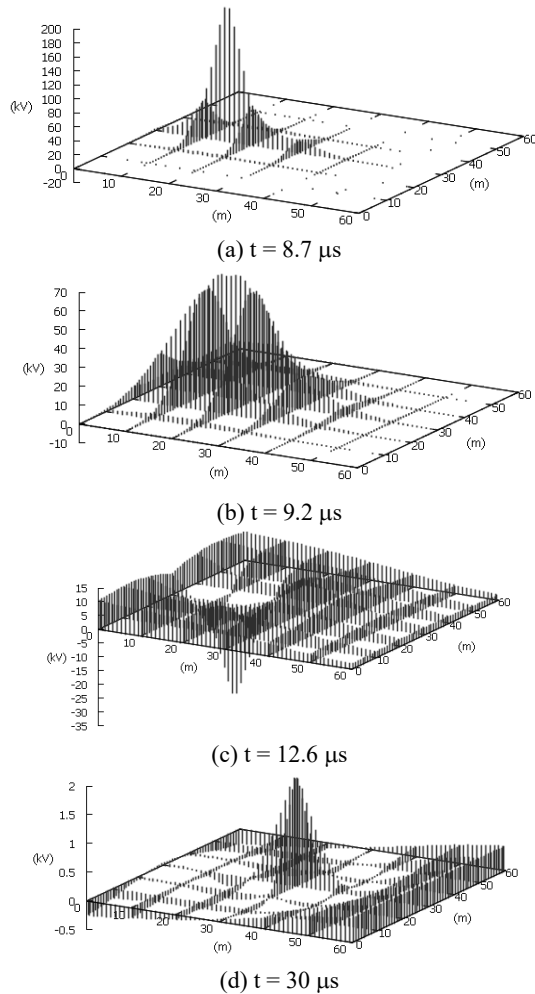


Fig. 21. Snapshots of computer animation of the potential distribution at grounding conductors computed by Tragsys for the case of lightning current of 30 kA 0.5/3 μ s and soil resistivity 100 Ω m.

Fig. 20 shows the currents injected into the grounding system for the case of lightning current of 30 kA 0.5/3 μ s and soil resistivity 100 Ω m at the arrester and at transformer grounding points. These currents are used to analyze the potential distribution in the ground as shown in Fig. 21. The resulting temporal and spatial distribution of the potential of ground grid conductors is presented as individual “snapshots” of the computer animation. It can be seen that in the first instants of the current injection in the grounding system, due to limited speed of propagation only smaller part of the grounding system is active in discharging current into soil, which results in very large potentials near the injection point. Complex propagation of potentials and induced voltages during transient period computed by described method are of interest in EMC studies of connected sensitive equipment.

VIII. CONCLUSION

This work presents a very accurate study of a complex grounding system behavior when large transformers are exposed to severe lightning conditions. It has been shown that the grounding impedance that depends on the grounding mesh structure and the soil resistivity plays an important role in the determination of the correct overvoltage values. The paper also demonstrates an efficient interface that is built in ATPDraw environment, and is based on a proven methodology. According to this methodology, when the connection points of the system above ground are known, and the self and mutual impedances for the predefined grounding system from these points are determined, the grounding system can be interfaced to the system above ground with full success. Ignoring grounding resistances and considering the earth as an ideal conductor, or predicting constant values for the grounding resistance may lead to very inaccurate results even though the system components above ground are modeled within broad frequency range. More work will be done in the future to show the effect of the grounding system when the lightning hits the overhead line ground wires (if they exist), and what the overvoltage values will be in case when a flashover takes place between overhead line conductors. This will require an extended application of this methodology that will take into account ground wires earthing.

IX. REFERENCES

- [1] IEEE std. 80-2000: *Guide for Safety in AC Substation Grounding*, IEEE Standard.
- [2] M. Mitolo: Of Electrical Distribution Systems with Multiple Grounded Neutrals, *Industry Applications, IEEE Transactions on* 46 (4), 1541-1546.
- [3] M Mitolo: Grounding the Neutral of Electrical Systems Through Low-Resistance Grounding Resistors: An Application Case, *Industry Applications, IEEE Transactions on* 44 (5), 1311-1316.
- [4] F Freschi, A Guerrisi, M Tartaglia, M Mitolo: Numerical Simulation of Heart-Current Factors and Electrical Models of the Human Body, *Industry Applications, IEEE Transactions on* 49 (5), 2290-2299.
- [5] ABB: <http://www.abb.com/product/db0003db004279/c125739900636470c125708c0041b9a9.aspx>
- [6] J. J. Grainger, W. D. Stevenson: *Power System Analysis*, McGraw-Hill International Edition.
- [7] E.D. Sunde: *Earth Conduction Effects in Transmission Systems*, New York, Dover Publication, 1968.
- [8] L. Grcev and F. Dawalibi, “An electromagnetic model for transients in grounding systems,” *IEEE Trans. Power Del.*, vol. 5, no. 4, pp. 1773–1781, Oct. 1990.
- [9] L. Grcev, “Computer analysis of transient voltages in large grounding systems,” *IEEE Trans. Power Del.*, vol. 11, no. 2, pp. 815–823, Apr. 1996.
- [10] TRAGSYS-Software for High Frequency and Transient Analysis of Grounding Systems. [Online]. Available: <http://www.tragsys.com>
- [11] R. F. Harrington, *Field Computation by Moment Methods*. New York: Wiley–IEEE, 1993.
- [12] M. Heimbach, L. Grcev, “Grounding system analysis in transients programs applying electromagnetic field approach,” *IEEE Transactions on Power Delivery*, vol. 12, no. 1, pp. 186-193, January 1997.
- [13] L. Grcev, M. Popov: On high-frequency circuit equivalents of a vertical ground rod, *IEEE Transactions on Power Delivery*, Vol. 20, No. 2, pp. 1598-1603, April 2005.
- [14] T. Noda, N. Nagaoka: Development of ARMA Models for Transient Calculation using linearized Least-square method, *IEEE transactions of Japan*, Vol. 114-B, No. 4, pp. 396-402, 1994.

- [15] T. Noda, N. Nagaoka, A. Ametani: Phase domain modeling of frequency transmission lines by means of an ARMA model, *IEEE Transactions on Power Delivery*, Vol. 11, No. 1, pp. 401-411, January 1996.
- [16] M. Kizilcay: Low-order network equivalent for electromagnetic transient studies, *European Transactions on electrical Power Engineering (ETEP)*, vol. 3, No. 2, pp. 123-129, March/April 1993.
- [17] B. Gustavsen, A. Semlyen: Rational Approximation of Frequency Domain Responses by Vector Fitting, *IEEE Transactions on Power Delivery*, Vol. 14, No. 3, pp. 1052-1061, July 1999.
- [18] B. Gustavsen: Computer Code for Rational Approximation of Frequency Dependent Admittance Matrices, *IEEE Transactions on Power Delivery*, Vol. 17, No. 4, pp. 1093-1098, October 2002.
- [19] ABB surge arresters – Buyers Guide, Edition 5.1, 2007-04.
- [20] <http://www.arresterworks.com/>
- [21] M. Popov, L. van der Sluis, G. C. Paap: "Investigation of the Circuit Breaker Reignition Overvoltages Caused by No-load Transformer Switching Surges", *European Transactions on Electric Power (ETEP)*, Vol. 11, No. 6, 2001, pp. 413-422.
- [22] B. Gustavsen, A.P. Brede, J.O. Tande: Multivariate Analysis of Transformer Resonance Overvoltages in Power Station, *IEEE Transactions on Power Delivery*, Vol. 26, Num. 4, 2011, pp.2563-2572.
- [23] C.L. Bak, K.E. Einarsdottir, E. Andresson, J.M. Rasmussen, J. Lykkegaard and W. Wiechowski: Overvoltage Protection of Large Power Transformers – A Real-Life Study Case, *IEEE Transactions on Power Delivery*, Vol. 23, No. 2, 2008, pp.657-666.



Bjørn Gustavsen (M'94–SM'2003–F'2014) was born in Norway in 1965. He received the M.Sc. degree and the Dr.Eng. degree in Electrical Engineering from the Norwegian Institute of Technology (NTH) in Trondheim, Norway, in 1989 and 1993, respectively. Since 1994 he has been working at SINTEF Energy Research where he is currently Chief Scientist. His interests include simulation of electromagnetic transients and modeling of frequency dependent effects. He spent 1996 as a Visiting Researcher at the University of Toronto, Canada, and the summer of 1998 at the Manitoba HVDC Research Centre, Winnipeg, Canada. He was a Marie Curie Fellow at the University of Stuttgart, Germany, August 2001–August 2002. He is convener of CIGRE JWG A2/C4.52.



Vladimir Terzija (M'95, SM'2000) is the EPSRC Chair Professor in Power System Engineering in the School of Electrical and Electronic Engineering, The University of Manchester, where he has been since 2006. From 1997 to 1999, he was an Associate Professor at the University of Belgrade. In 1999, he was awarded a Humboldt Research Fellowship. From 2000 to 2006, he was with ABB, Germany, working as an expert for switchgear and distribution automation. His main research interests are application of intelligent methods to power system monitoring, control, and protection, switchgear and fast transient processes, as well as DSP applications in power.

X. BIOGRAPHIES



Marjan Popov (M'95, SM'2003) obtained his Dipl.-Ing. degree from the Ss. Cyril and Methodius University, Skopje, Macedonia in 1993 and the Ph.D degree in Electrical Power Engineering from Delft University of Technology in 2002, The Netherlands. Currently he is Associate Professor in Electrical Power Engineering at TU Delft. In 2010, he obtained the prestigious Dutch Hidde Nijland award for extraordinary research achievements in the field of Electrical Power Engineering in the Netherlands. He is also IEEE PES Prize Paper Award and IEEE Switchgear Committee Award recipient for 2011. His major fields of interest are in large scale of power system transients, intelligent protection for power systems and wide area monitoring and protection. He is a member of Cigre and Dutch national SC B5 and actively participated in Cigre JWG C4.402 and JWG A2/C4.39 as well as Cigre JWG A2/C4.52.



Leonid Greev (M'84–SM'97–F'13) is a professor with the Faculty of Electrical Engineering and Information Technologies at the Ss. Cyril and Methodius University, Skopje, Macedonia, where he has been since 1988. From 1978 to 1988, he was with the Electric Power Company of Macedonia. He has been a Visiting Professor at the Technical University of Aachen, Germany, Eindhoven University of Technology, The Netherlands and the Swiss Federal Institute of Technology, Lausanne, Switzerland. He is the principal author of TRAGSYS software for transient analysis of grounding systems. He is a Member of Macedonian Academy of Sciences and Arts.



Hans Kr. Høidalen (M'05–SM'14) was born in Norway in 1967. He received the M.Sc. and Ph.D. degrees from the Norwegian University of Science and Technology, Trondheim, in 1990 and 1998, respectively. He is now a Professor at the same institution with a special interest of power system transients, lightning and electrical stress calculations. In recent years the focus has been on transformer analysis and power system protection. He is the developer of the pre-processor to EMTP-ATP called ATPDraw.